RSC Advances

PAPER

View Article Online
View Journal | View Issue

Cite this: *RSC Adv.*, 2018, **8**, 18966

Nitrogen and sulfur co-doped graphene aerogel for high performance supercapacitors†

Zhiwei Lu,‡ Yujuan Chen,‡ Zhaoen Liu, Aoqi Li, Dong Sun and Kelei Zhuo *

Received 27th February 2018
Accepted 16th May 2018

DOI: 10.1039/c8ra01715h

rsc.li/rsc-advances

The development of high energy density and power density supercapacitors is very necessary in energy storage and application fields. A key factor of such devices is high-performance electrode materials. In this work, nitrogen and sulfur co-doped graphene aerogels (N/S-GA) were synthesized using graphene oxide as the precursor and 2-mercapto-1-methylimidazole as both the reducing agent and the N/S doping agent. The pore size distribution of the as-prepared N/S-GA was measured and the N/S-GA possesses a hierarchical porous structure. As an electrode material of supercapacitors, the N/S-GA could provide a suitable structure for charge accommodation and a short distance for ion transport. When 1-ethyl-3-methylimidazolium tetrafluoroborate ([Emim]BF_4) ionic liquid was used as the electrolyte, the specific capacitance of the N/S-GA electrode material reached 212 F g^{-1} and 162 F g^{-1} at the current densities of 1 A g^{-1} and 10 A g^{-1}, respectively. And the energy density and average power density of the N/S-GA based supercapacitor could reach 117 W h kg^{-1} and 1.0 kW kg^{-1} at 1 A g^{-1}, 82 W h kg^{-1} and 9.5 kW kg^{-1} at 10 A g^{-1}, respectively. It is believed that the N/S-GA material can be used in high-performance supercapacitors.

Introduction

With the fast-increasing market of electric vehicles and electronic devices, great efforts have been made for developing efficient and clean electrochemical energy storage devices.[1,2] Electrochemical double layer capacitors (EDLCs), also called supercapacitors, are applicable in many fields due to their fast charge–discharge rates, high power density, long cycle life, and high safety.[3–5] In general, the main electrode materials of EDLCs are carbon materials, such as activated carbon, carbon nanotubes, mesoporous carbon, and graphene.[6–8]

Graphene, a flat sheet of carbon with one atom thickness, has many excellent properties such as light weight, high stability, high conductivity, and high specific surface area,[9] and thus has potential to fabricate high-performance supercapacitors. However, graphene has some inevitable problems that limit its practical application to supercapacitors. For example, graphene sheets would be re-stacked during the production process, resulting in the small pore sizes in the graphene be insufficiently accessible to the electrolyte.[10] The specific capacitance of graphene is generally in the range of 100–200 F g^{-1}, which is far lower than its theoretical value of 550 F g^{-1}.[11] A strategy to increase the specific capacitance of graphene is to introduce heteroatoms into its lattice. When carbon atoms in the graphene lattice are partly substituted with heteroatoms, the capacitive performance of the materials can be improved. Incorporation of heteroatoms into graphene can tailor its electron donor properties, and accordingly regulate the electrical and chemical performances of the surface.[12] Consequently, this can decrease the charge transfer resistance, improve the surface wettability, and enhance the capacitive performance.[9] The heteroatoms, such as N, S, P and B, can modify graphene by either single or dual doping.[13–16] The single heteroatom doping can merely enhance one aspect of the properties, and the co-doping can improve many performances of graphene due to their synergetic effect.[17,18] For instance, Yu *et al.* studied the synergistic effect of heteroatoms co-doped graphene.[19] Kotal *et al.*[20] prepared sulfur and nitrogen co-doped holey graphene aerogel, which exhibited significantly high volumetric capacitance (203 mF cm^{-3}) in the structurally resilient solid-state supercapacitors.

In addition to the electrode materials, the electrolyte also plays an important role in the performance of supercapacitors. A variety of ionic liquids have been studied as the electrolyte because of their wider electrochemical window than water and organic solvents.[21–24] For example, 1-ethyl-3-methylimidazolium tetrafluoroborate ([Emim]BF_4) has a relative wide electrochemical window and high electrical conductivity, and thus is a promising electrolyte for fabricating high-performance supercapacitors.[25] Tian *et al.*[26] prepared graphene-like nitrogen-doped carbon nanosheets as electrode materials and

Collaborative Innovation Center of Henan Province for Green Manufacturing of Fine Chemicals, Key Laboratory of Green Chemical Media and Reactions, Ministry of Education, School of Chemistry and Chemical Engineering, Henan Normal University, Xinxiang, Henan 453007, P. R. China. E-mail: klzhuo@263.net

† Electronic supplementary information (ESI) available. See DOI: 10.1039/c8ra01715h

‡ Both authors contributed equally to this work.

used mixed ionic liquids as electrolyte; the specific capacitance of the electrode materials was 162 F g^{-1}. Huang *et al.*[27] used hierarchical porous graphene carbon as electrode materials and [Emim]BF_4 as electrolyte to construct supercapacitors; the specific capacitance of the electrode materials reached 196 F g^{-1}. Song *et al.*[28] synthesized diamine/triamine functionalized graphene networks as electrode materials in [Emim]BF_4 electrolyte, and the specific capacitance of the electrode materials was 119 F g^{-1}. Yu *et al.*[19] synthesized P/S co-doped graphene aerogels as electrode materials and used [Bmim]BF_4 as the electrolyte to prepare the supercapacitor; the specific capacitance of the aerogels was 208 F g^{-1}. Therefore, the EDLCs with heteroatoms co-doped graphene as the electrode material and ionic liquids as the electrolyte are a type of potential devices for energy storage and application.

Herein, we report a one-step hydrothermal self-assembly method for synthesizing novel nitrogen and sulfur co-doped graphene hydrogels (N/S-GH), which were then freeze-dried to obtain N/S-GA. The N/S-GA prepared under optimum conditions possessed mesopores and macrospores, and thus had rich electrochemical activity sites and defects. These features endowed the as-prepared N/S-GA with remarkable capacitive properties: a specific capacitance of 212 F g^{-1} at 1 A g^{-1}. And the N/S-GA based supercapacitor showed a high energy density of 117 W h kg^{-1} at 1 A g^{-1}.

Experimental

Synthesis of the GA and N/S-GA-*x*

Graphene oxide (GO) was synthesized from graphite (Aladdin reagent Inc, Shanghai, China) using the modified Hummers' method.[29] GH and N/S-GH was obtained by the hydrothermal synthesis method and then was freeze-dried to obtain GA and N/S-GA. Briefly, different masses of 2-mercapto-1-methylimidazole (Aladdin Reagent Inc, Shanghai, China) were added respectively into an aqueous solution (40 mL, 1 mg mL^{-1}) of graphene oxide (GO) and ultrasonically treated for 10 min. Then the mixture was transferred to a 100 mL Teflon lined autoclave and reacted at 200 °C for 12 hours. After cooling to room temperature, the obtained hydrogels were washed with deionized water, and then were dialyzed against water using dialysis membranes (retained molecular weight: 500 Da) for 72 h to remove impurities (deionized water was renewed once a day). The resulting samples were named as GA (the mass ratio of 2-mercapto-1-methylimidazole to the GO is 0.1) and N/S-GA-*x* (*x* is the mass ratio of 2-mercapto-1-methylimidazole to the GO, $x = 0.5, 1, 2, 5$).

Characterization

The morphologies of the N/S-GA-2 were analyzed using transmission electron microscopy (TEM, JEOL JEM-2100) and field-emission scanning electron microscopy (FESEM, Zeiss Supra 40). The structures were characterized by X-ray diffraction (XRD, Bruker D8 Advance) and Renishaw Raman spectrometer. And X-ray photoelectron spectroscopy (XPS, ESCALab220i-XL) spectra were recorded to analyze the chemical composition of the materials. N_2 adsorption/desorption isotherms were measured on a Micromeritics ASAP 2020. The Brunauer–Emmett–Teller (BET) method was used to obtain the specific surface area. The pore size distribution was obtained using the Barrett–Joyner–Halenda (BJH) model.

Experimental measurements

The active material (GA or N/S-GA-*x*), acetylene black, and polytetrafluoroethylene were mixed at a mass ratio of 85 : 10 : 5 in ethanol to form a mixture. The mixture was ultrasonicated for about 30 min to obtain homogenous slurry. The slurry was pressed onto the nickel foam and transferred to a vacuum drying oven at 110 °C for 8 h, and then the treated nickel foam was pressed with a pressure of 10 MPa. The mass of the active material on every electrode was about 1.2 mg.

The test cell was a symmetrical two-electrode system with [Emim]BF_4 as electrolyte. The punched electrode discs as both the positive and negative electrodes were assembled in CR2032 coin cells. The assembling processes were operated in a glove box. The electrochemical impedance spectra (EIS), galvanostatic charge–discharge (GCD), and cyclic voltammetry (CV) measurements were performed on a CHI660D electrochemical working station (Shanghai Chenhua instrument Co., Ltd., China). The potentiostat/galvanostat tests were conducted on a CT2001A battery test system (Lanhe, Wuhan, China).

The capacitance (C) of a cell (supercapacitor) is calculated from the slope of the galvanostatic discharge curve (eqn (1)):

$$C = \frac{I \times \Delta t}{\Delta U} \quad (1)$$

where I is the discharge current (A), Δt is the discharge time (s), and ΔU is the change in cell potential (V, excluding ohmic drop IR). The specific capacitance of single electrode (C_{sp}, F g^{-1}) is calculated from eqn (2):[9]

$$C_{sp} = \frac{2C}{0.5m} \quad (2)$$

where m is the total mass of N/S-GA in two electrodes (a cell) (g). The energy density (E, W h kg^{-1}) and average power density (P, kW kg^{-1}) of the supercapacitor are calculated from the eqn (3) and (4):[26]

$$E = \frac{C \times \Delta U^2}{2 \times m \times 3.6} \quad (3)$$

$$P = \frac{3600E}{\Delta t} \quad (4)$$

Results and discussion

The morphologies of the N/S-GA-2 were investigated by FESEM and TEM (Fig. 1). Fig. 1a, the N/S-GA-2 shows a 3D framework of graphene sheets with macrospores. The distributions of nitrogen and sulfur in the N/S-GA-2 are in Fig. S3.† The TEM image of the N/S-GA-2 (Fig. 1b) reveals the crinkled structure and fewer layers of graphene sheets. And the FESEM and TEM images also indicate that the N/S-GA-2 contained hole defect

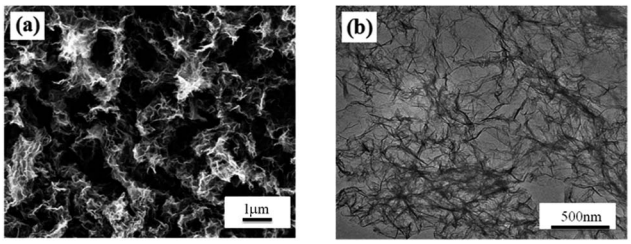

Fig. 1 FESEM image (a) and TEM image (b) of the N/S-GA-2.

graphene sheets. The crinkled structure may be caused by the N and S modified graphene lattices.

The porosity of the N/S-GA-2 was analyzed by nitrogen adsorption/desorption isotherms. Fig. 2a shows the type IV isotherm with an obvious hysteresis loop, indicating the existence of mesoporous in the N/S-GA-2.[30] The isotherm of the N/S-GA-2 shows a sharp uptake at relative pressures of 0.9–1.0, which is attributed to the plenty of textural macropores in the N/S-GA-2.[31] The porous size distribution curve calculated by using the BJH method shows the presence of hierarchical pores in the N/S-GA-2 (Fig. 2b). And the proportion of macropores distribution with a peak pore diameter of approximately 120 nm is relatively higher than those of other pore diameters. This indicates that the N/S-GA-2 based supercapacitors can be charged and discharged fastly, and thus may possess a superior rate capability.[30] The Brunauer–Emmett–Teller (BET) specific surface area of the N/S-GA-2 was 181 $m^2\ g^{-1}$.

The XRD patterns of GO and N/S-GA-2 are shown in Fig. 3. The GO pattern exhibits a sharp diffraction peak at $2\theta = 9.9°$, which is ascribed to the crystalline plane of GO.[21] However, this peak completely disappeared and a diffraction peak appeared at 24.8° for the N/S-GA-2, suggesting that GO was well conversed to graphene.[32–35] The peak of the N/S-GA-2 at 24.8° is relatively weak and broad, indicating that grapheme sheets were much disordered. This may be attributed to the formation of defects and vacancies caused by heteroatom doping.

The chemical composition of the GA and N/S-GA-2 was investigated by XPS. The results show that atomic percentages of elements in the N/S-GA-2 were 86.36% C, 2.77% N, 10.99% O, and 0.89% S. The GA had no S and N, and the contents (atomic percentage) of N and S elements in N/S-GA-x (x = 0.5, 1, 2, 5) were 2.03% and 0.6%, 2.5% and 0.74%, 2.77% and 0.89%, and 3.83% and 1.22%, respectively. Fig. 4a shows the full XPS spectrum of the N/S-GA-2, and three main characteristic peaks are observed at 286.3 eV (C1s), 402.8 eV (N1s), and 534.9 eV

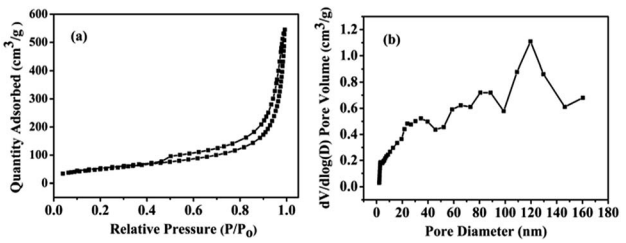

Fig. 2 N_2 adsorption/desorption isotherm (a) and pore size. Distribution of the N/S-GA-2 (b).

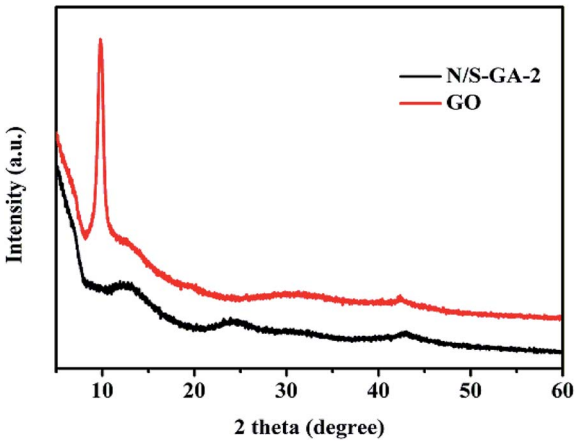

Fig. 3 XRD patterns of the GO and N/S-GA-2.

(O1s), respectively. There is also a weak peak at 165.1 eV, corresponding to S2p. The results indicate that the nitrogen and sulfur were successfully doped into graphene lattice. The S2p can be deconvoluted into four peaks at binding energies of 165.4 eV, 166.0 eV, 167.9 eV, and 169.3 eV (Fig. 4b). The peak at 165.4 eV is corresponding to S2p1/2. The peaks at 166.0 eV, 167.9 eV and 169.3 eV are deemed to be different oxidized sulfur forms of C–SO_x–C (x = 2–4) bonds.[9,14,36] S2p1/2 of the C–SO_x–C covalent bonds corresponds to the thiophene-S that is caused by spin–orbit coupling.[14] And the C–SO_x–C bonds are usually formed at the edge of graphene.[37] The results indicate that there are a plenty of hole defective graphene sheets in the N/S-GA-2. The high resolution N1s spectrum only has one peak at 402.4 eV (Fig. 4c), corresponding to the pyridine-*N*-oxide group.[38] Thus, we can speculate that the formation of C–SO_x–C and N–O bonds is ascribed to the redox reactions between the oxygen-containing groups of GO and 2-mercapto-1-methylimidazole.

Fig. 4d shows the Raman spectra of the N/S-GA-2 and GO, with two wide peaks at 1340 cm^{-1} and 1585 cm^{-1}

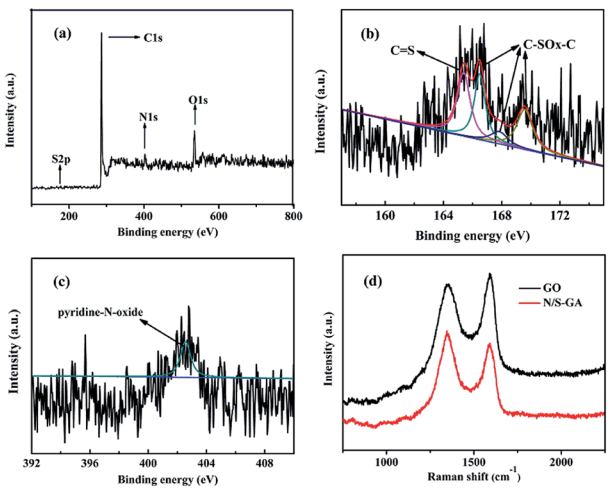

Fig. 4 XPS scanning spectrum of the N/S-GA-2 (a), high resolution XPS spectra of S2p (b) and N1s (c), and Raman spectra of the N/S-GA-2 and GO (d).

corresponding to the typical D and G bands, respectively.[39] The D band corresponds to the degree of disorder in structure and the G band associates with the first order scattering vibration of sp2 hybridized carbon atoms.[26] The intensity ratio of D to G bands (I_D/I_G) was used to analyze the amount of structure defects.[32] And the I_D/I_G value for the N/S-GA-2 is 1.03, which is larger than that for GO, indicating that the N/S-GA-2 had more defects on the graphene sheets. Consequently, the N/S-GA-2 based supercapacitor can storage more ions. It may be ascribed to the substitution of C atoms with N and S atoms.[40]

Next, we studied the performances of the supercapacitor based on GA and N/S-GA-*x* as the electrode materials and [Emim]BF_4 as the electrolyte. Fig. 5a illustrates CV curves of GA and N/S-GA-*x* electrodes. The loop area of the N/S-GA-2 had the maximum value, which corresponds to the largest specific capacitance. We further investigated the GCD performances of the GA and N/S-GA-*x* electrode (Fig. 5b). At the current density of 2 A g^{-1}, the specific capacitance values were 138, 177, 169, 201, and 180 F g^{-1} for GA and N/S-GA-*x* (x = 0.5, 1, 2, and 5), respectively, showing that the N/S-GA-2 electrode had the largest specific capacitance. Therefore, we further investigated other electrochemical performances of the N/S-GA-2.

Fig. 6a shows the CV curves of the N/S-GA-2 electrode at different scan rates. It can be seen that all the CV curves are closed to the perfect rectangular loop and have a redox peak, indicating that the charge storage mechanism is of the electrical double-layer capacitance and pseudocapacitance,[41] and the electrical double-layer capacitance contribution is far greater than the pseudocapacitance. The CV curves remain the rectangular loop even at the scan rate up to 200 mV s^{-1}, showing an excellent rate capability. It may be due to the vast macropores in the N/S-GA-2, and the macropores could make the electrolyte ions to get into/out the electrode quickly. The oxidation peak (1.3–1.7 V) in Fig. 6a showed a polarization process, which was caused by the redox reactions of nitrogen, sulfur, and residual oxygen-containing functional groups in N/S-GA-2. In the process of charging and discharging, the redox reactions would contribute a pseudocapacitance to the supercapacitor. GCD tests were used to further study electrochemical performances of the N/S-GA-2 electrode. Fig. 6b shows charge/discharge curves at current densities from 1 A g^{-1} to 10 A g^{-1}. All the curves are nearly linear and symmetric, indicating the ideal electrical double-layer capacitance performance. The variation of the specific capacitances at different current densities is

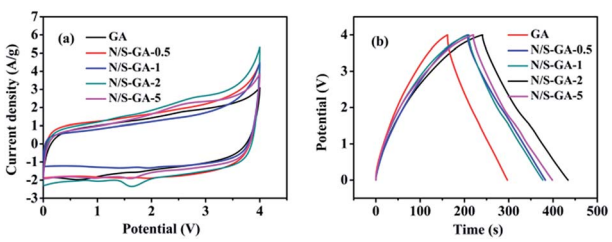

Fig. 5 Electrochemical performances of N/S-GA-*x* electrode (x = 0.1, 0.5, 1, 2, 5): (a) CV curves at 20 mV s^{-1}, (b) GCD curves at current density of 2 A g^{-1}.

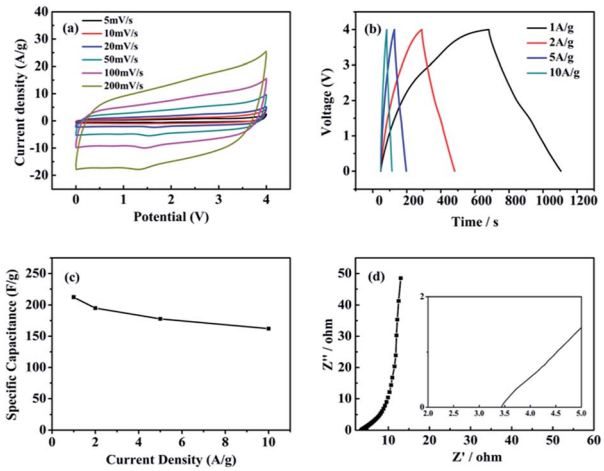

Fig. 6 Electrochemical performance of the N/S-GA-2 electrode in the [Emim]BF_4 electrolyte: (a) CV curves at different scan rates, (b) GCD curves at different current densities, (c) specific capacitances at different current densities, (d) the Nyquist plots of supercapacitor (the inset is Nyquist plots showing the imaginary part *vs.* the real part of impedance).

shown in Fig. 6c. The specific capacitance values of N/S-GA-2 were 212, 195, and 178 F g^{-1} at 1, 2, and 5 A g^{-1}, respectively. And even at a current density of 10 A g^{-1}, the specific capacitance was also up to 162 F g^{-1}, showing an excellent rate capability (the capacitance maintains 76.3% when the current density expands 10 times). The specific capacitance of the N/S-GA-2 at a current density of 1 A g^{-1} in [Emim]BF_4 was higher than that of the graphene aerogel in 5 M KOH (160 F g^{-1} at 1 A g^{-1}),[42] and slightly less than that of the N-doped graphene aerogel in 1.0 mol L^{-1} H_2SO_4 (223 F g^{-1} at 0.2 A g^{-1}).[43] For comparison, some graphene composites materials and the supercapacitors based on these materials in ionic liquids were collected in Table 1. The specific capacitance of the N/S-GA-2 and the energy density of the N/S-GA-2 based supercapacitor in this work are maximal. This can be interpreted according to the structure characteristics of the materials. First, the excellent electrochemical performances of N/S-GA-2 should be attributed to its network structure and the sulfur and nitrogen co-doping. The network structure with hole structure defective may offer abundant ion-accessible surfaces, and the N/S co-doping can provide much electrochemical active sites. Thus, the wettability and electrical conductivity of the electrode material can increase effectively. Second, the N/S-GA-2 contained hierarchical porous structure. The macropores decrease the diffusion distance of the electrolyte ions to each pore, and the micropores and mesopores provide large accessible surface area for the charge accommodation and ion transport. The specific surface area of the N/S-GA-2 can be used sufficiently. Consequently, even if the specific surface area of the N/S-GA-2 was 181 m^2 g^{-1}, it would exhibit an excellent electrochemical performance.

The specific capacitances reduced gradually with increasing current densities (Fig. 6c), which can be attributed to the fact that the electrolyte ions have no sufficient time to diffuse into the entire pores.[44] The voltage drops at the beginning of the

Table 1 Summary of electrochemical performances of some graphene composites electrode materials and the supercapacitors based on the materials in ionic liquids as the electrolyte

Electrode materials	Electrolyte	ES[a]	SC[b]	E^c	Reference
Sulfur/phosphorus co-doping porous graphene aerogel	[Bmim]PF_6	Three	208	88.5	19
Graphene-like nitrogen-doped carbon nanosheets	[Emim]TFSI/[Emim]BF_4	Two	162	51	25
Hierarchical porous graphene carbon	[Emim]BF_4	Two	196	83.1	26
Diamine/triamine functionalized graphene networks	[Emim]BF_4	Two	119	51	27
Nitrogen and sulfur co-doped graphene aerogel	[Emim]BF_4	Two	212	117	Current work

[a] Electrode system. [b] Specific capacitance (F g^{-1}). [c] Energy density (W h kg^{-1}).

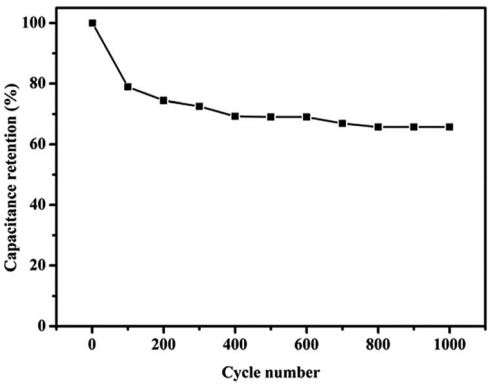

Fig. 7 Capacitance retentions *vs.* cycle numbers at the current density of 1 A g^{-1}.

discharge are 0.019, 0.038, 0.091, and 0.176 V at 1, 2, 5, 10 A g^{-1}, respectively, indicating that the equivalent series resistance (R_s, a sum of the intrinsic resistance of the material, the ionic resistance of [Emim]BF_4, and the contact resistance between the nickel foam and the material) of the supercapacitor was very low, and thus the capacitive performance was excellent.

Electrochemical impedance spectroscopy (EIS) was used to further understand the electronic and ionic transport process.[26] Fig. 6d shows the Nyquist plot by the frequency response analysis at the frequency range from 100 kHz to 1 Hz. The R_s value was calculated from the high frequency region truncation of the plot by the real axis.[22] The obtained value was 3.4 Ω, indicating the N/S-GA-2 had a low internal resistance and good conductivity.[45] The lack of obvious semicircle in the high frequency indicates that the charge transfer resistance (R_{ct}) was low.[46] The result is in agreement with those from the CV and charge/discharge analyses. The values of both R_{ct} and R_s were very small, further indicating a highly effective ion-diffusion and charge-transfer in the N/S-GA-2, and thus the supercapacitor had an excellent rate capability.[23,47] In addition, the N/S-GA-2 based supercapacitor exhibited the capacitance retention of 66.3% after 1000 cycles at the current density of 1 A g^{-1} (Fig. 7).

The energy densities (E) calculated from eqn (3) were 117, 106, 94, and 82 W h kg^{-1} at the current densities of 1, 2, 5, and 10 A g^{-1}, respectively, and average power densities (P) calculated from eqn (4) were 1.0, 2.0, 4.9, and 9.5 kW kg^{-1} at the corresponding current densities. This indicates that the supercapacitor can provide a large energy density of 82.0 W h kg^{-1} even at a high average power density of 9.5 kW kg^{-1}. In addition, Table 1 shows that the energy density value of the supercapacitor is more than those of the graphene-based supercapacitors reported previously.[19,26–28]

Conclusions

In summary, sulfur and nitrogen co-doped graphene aerogel was synthesized by chemical reduction of GO using 2-mercapto-1-methylimidazole as both the reducing agent and the doping agent. The as-prepared N/S-GA-2 possessed hierarchical porous structures, which is beneficial to charge accommodation and the ion diffusion. Meanwhile, the structure of the N/S-GA-2 also had a plenty of electrochemical active sites which can also significantly enhance its electrochemical performances. The N/S-GA-2 material exhibited a high specific capacitance of 212 F g^{-1}, and the N/S-GA-2 based supercapacitor with [Emim]BF_4 as the electrolyte showed a high energy density of 117 W h kg^{-1} at 1 A g^{-1}, and had a high energy density of 82.0 W h kg^{-1} even at a high average power density of 9.5 kW kg^{-1}. We believe that the N/S-GA-2 is a potential electrode material for high-performance supercapacitors.

Conflicts of interest

There are no conflicts to declare.

Acknowledgements

Financial supports from the National Natural Science Foundation of China (No. 21573058, 21303044, 21173070), Program for Innovative Research Team in Science and Technology in University of Henan Province (15IRTSTHN 003, 17IRTSTHN 001) are gratefully acknowledged.

Notes and references

1 J. R. Miller and P. Simon, *Science*, 2008, **321**, 651–652.
2 P. Simon and Y. Gogotsi, *Nat. Mater.*, 2008, **7**, 845–854.
3 D. X. Du, Q. X. Bian, J. B. Zhang and X. H. Yang, *RSC Adv.*, 2017, **7**, 46329–46335.
4 S. Ramesh, A. Sivasamy, H. S. Kim and J. H. Kim, *RSC Adv.*, 2017, **7**, 49799–49809.
5 M. Demir, S. K. Saraswat and R. B. Gupta, *RSC Adv.*, 2017, **7**, 42430–42442.

6 Q. Long, W. Chen, H. Xu, X. Xiong, Y. Jiang, F. Zou, X. Hu, Y. Xin, Z. Zhang and Y. Huang, *Energy Environ. Sci.*, 2013, **6**, 2497–2504.
7 K. H. An, W. S. Kim, Y. S. Park, J. M. Moon, D. J. Bae, S. C. Lim, Y. S. Lee and Y. H. Lee, *Adv. Funct. Mater.*, 2001, **11**, 387–392.
8 C. Liu, Z. Yu, D. Neff, A. Zhamu and B. Z. Jang, *Nano Lett.*, 2014, **10**, 4863–4868.
9 N. Q. Tran, B. K. Kang, M. H. Woo and D. H. Yoon, *ChemSusChem*, 2016, **9**, 2261–2268.
10 K. F. Chen, S. Y. Song, F. Liu and D. F. Xue, *Chem. Soc. Rev.*, 2015, **44**, 6230–6257.
11 J. Xia, F. Chen, J. Li and N. Tao, *Nat. Nanotechnol.*, 2009, **4**, 505–509.
12 Y. Li, G. Wang, T. Wei, Z. Fan and P. Yan, *Nano Energy*, 2016, **19**, 165–175.
13 D. Hulicova-Jurcakova, A. M. Puziy, O. I. Poddubnaya, F. Suárez-García, J. M. Tascón and G. Q. Lu, *J. Am. Chem. Soc.*, 2009, **131**, 5026–5027.
14 Y. Huang, S. L. Candelaria, Y. Li, Z. Li, J. Tian, L. Zhang and G. Cao, *J. Power Sources*, 2014, **252**, 90–97.
15 Y. P. Wu, S. Fang, Y. Jiang and R. Holze, *J. Power Sources*, 2002, **108**, 245–249.
16 C. Jackson, M. Shahsahebi, T. Wedlake and C. A. Dubard, *Energy Environ. Sci.*, 2013, **6**, 2465–2476.
17 D. Hulicova-Jurcakova, M. Seredych, Q. L. Gao, N. K. A. C. Kodiweera, P. E. Stallworth, S. Greenbaum and T. J. Bandosz, *Carbon*, 2009, **47**, 1576–1584.
18 S. Wang, E. Iyyamperumal, A. Roy, Y. Xue, D. Yu and L. Dai, *Angew. Chem., Int. Ed.*, 2011, **50**, 11756–11760.
19 X. Yu, Y. Kang and H. S. Park, *Carbon*, 2016, **101**, 49–56.
20 M. Kotal, H. Kim, S. Roy and K. Oh, *J. Mater. Chem. A*, 2017, **5**, 17253–17266.
21 M. Armand, F. Endres, D. R. Macfarlane, H. Ohno and B. Scrosati, *Nat. Mater.*, 2009, **8**, 621–629.
22 K. P. Gong, S. Chakrabarti and L. M. Dai, *Angew. Chem., Int. Ed.*, 2008, **47**, 5446–5450.
23 R. Kötz and M. Carlen, *Electrochim. Acta*, 2000, **45**, 2483–2498.
24 M. Vijayakumar, B. Schwenzer, V. Shutthanandan, J. Z. Hu, J. Liu and I. A. Aksay, *Nano Energy*, 2014, **3**, 152–158.
25 S. J. Zhang, N. Sun, X. Z. He, X. M. Lu and X. P. Zhang, *J. Phys. Chem. Ref. Data*, 2006, **35**, 1475–1517.
26 W. Tian, Q. Gao, L. Zhang, C. Yang, Z. Li, Y. Tan, W. Qian and H. Zhang, *J. Mater. Chem. A*, 2016, **4**, 8690–8699.
27 J. Huang, J. Wang, C. Wang, H. Zhang, C. Lu and J. Wang, *Chem. Mater.*, 2015, **27**, 2107–2113.
28 B. Song, J. Zhao, M. Wang, J. Mullavey, Y. Zhu, Z. Geng, D. Chen, Y. Ding, K. S. Moon and M. Liu, *Nano Energy*, 2017, **31**, 183–193.
29 D. Sun, L. Jin, Y. Chen, J. R. Zhang and J. J. Zhu, *ChemPlusChem*, 2013, **78**, 227–234.
30 Q. Shao, J. Tang, Y. Lin, J. Li, F. Qin, J. Yuan and L. C. Qin, *J. Power Sources*, 2015, **278**, 751–759.
31 Q. Chen, Y. Hu, C. Hu, H. Cheng, Z. Zhang, H. Shao and L. Qu, *Phys. Chem. Chem. Phys.*, 2014, **16**, 19307–19313.
32 D. Liu, C. Fu, N. Zhang, H. Zhou and Y. Kuang, *Electrochim. Acta*, 2016, **213**, 291–297.
33 D. Papkov, A. Goponenko, O. C. Compton, Z. An, A. Moravsky, X. Z. Li, S. B. T. Nguyen and Y. A. Dzenis, *Adv. Funct. Mater.*, 2013, **23**, 5763–5770.
34 S. Hwang, S. Lee and J. S. Yu, *Appl. Surf. Sci.*, 2007, **253**, 5656–5659.
35 D. Long, W. Li, L. Ling, J. Miyawaki, I. Mochida and S. H. Yoon, *Langmuir*, 2010, **26**, 16096–16102.
36 Y. J. Li, G. L. Wang, T. Wei, Z. J. Fan and P. Yan, *Nano Energy*, 2016, **19**, 165–175.
37 N. Parveen, M. O. Ansari, S. A. Ansari and M. H. Cho, *J. Mater. Chem. A*, 2016, **4**, 233–240.
38 J. Zhao, H. W. Lai, Z. Y. Lyu, Y. F. Jiang, K. Xie, X. Z. Wang, Q. Wu, L. J. Yang, Z. Jin, Y. W. Ma, J. Liu and Z. Hu, *Adv. Mater.*, 2015, **27**, 3541–3545.
39 D. Geng, S. Yang, Y. Zhang, J. Yang, J. Liu, R. Li, T. K. Sham, X. Sun, S. Ye and S. Knights, *Appl. Surf. Sci.*, 2011, **257**, 9193–9198.
40 Z. Jiang, X. Zhao, X. Tian, L. Luo, J. Fang, H. Gao and Z. J. Jiang, *ACS Appl. Mater. Interfaces*, 2015, **7**, 19398–19407.
41 Y. Wang, Z. Shi, Y. Huang, Y. Ma, C. Wang, M. Chen and Y. Chen, *J. Phys. Chem. C*, 2009, **113**, 13103–13107.
42 Y. X. Xu, K. X. Sheng, C. Li and G. Q. Shi, *ACS Nano*, 2010, **4**, 4324–4330.
43 Z. Y. Sui, Y. N. Meng, P. W. Xiao, Z. Q. Zhao, Z. X. Wei and B. H. Han, *ACS Appl. Mater. Interfaces*, 2015, **7**, 1431–1438.
44 C. Long, X. Chen, L. Jiang, L. Zhi and Z. Fan, *Nano Energy*, 2015, **12**, 141–151.
45 J. G. Wang, Y. Yang, Z. H. Huang and F. Kang, *Carbon*, 2013, **61**, 190–199.
46 Y. Guo and D. A. Rockstraw, *Microporous Mesoporous Mater.*, 2007, **100**, 12–19.
47 W. J. Qian, F. X. Sun, Y. H. Xu, L. H. Qiu, C. H. Liu, S. D. Wang and F. Yan, *Energy Environ. Sci.*, 2014, **7**, 379–386.